HyperXite
Research & Development

Ethan Leong
emleong1@uci.edu

- Simulation Modeling
- Model Dimensioning

Tae Rugh
rught@uci.edu

- Analytical Modeling
- Manufacturing Plan

MAE 189: Capstone Design
Winter 2022
University of California, Irvine
Professor Roger Rangel
February 15, 2022

Executive Summary

The Hyperloop pod is a vehicle that is set to revolutionize the technological advancement of transportation systems. Like the bullet train, it is meant to transverse from point A to B at a tremendous speed, making it convenient for people that rely on transportation systems for traveling and commuting. However, the Hyperloop pod is designed to travel through a vacuum tube to negate air friction so that the pod can achieve high accelerations. Ideally, the concept compensates the practical modes of transportation by being relatively inexpensive compared to airfares and fast compared to public transportation methods.

This year, HyperXite will be competing in European Hyperloop Week (EHW), a competition for Hyperloop teams to compete for awards for their Pod's mechanical, electrical, propulsion, and levitation systems, in addition to Pod completeness and scalability. However, beyond Pod performance, EHW has included a new Research Submission as part of the competition, designed to highlight Hyperloop-related research findings; this addition highlights EHW's desire to spotlight not only current technical achievements in the Hyperloop technology but also future potential developments.

Similarly, as a Senior Design Project as part of the Henry Samueli School of Engineering at UC Irvine, one of our major goals is to promote student learning through the work that we do, especially since our team includes students of different engineering disciplines, such as Mechanical, Aerospace, Electrical, and Computer Engineering. We encourage our members to explore designs and topics that interest them, allowing them to expand their knowledge in their personal areas of interest and discover potential new methodologies to improve our Pod.

For the past seven years, HyperXite has been working on the development of a small-scale hyperloop pod for the purpose of researching and developing the propulsion, braking, stabilization, and electronic systems aspects of Hyperloop. Our long-term objective is to align the development of our technology with the full-scale application of Hyperloop. To achieve this implementation goal, we account for conceptual and design considerations that would be important for the feasibility of high-speed, vacuum tunnel transportation, such as minimizing pod footprint to increase aerodynamics and efficiency. Other important considerations include maximizing the acceleration phase and minimizing braking distance to advance the Hyperloop's high-speed capabilities. Optimizing speed through current-to-power consumption and reducing latencies in our networking to enhance reliability. A recent effort on our team to achieve this goal is the development of a double-sided Linear Induction Motor for increasing thrust capabilities and decreasing friction losses.

Our goal to develop technology directly applicable to the Hyperloop concept is iterative in nature and is a result of prototype development, design analysis, and testing metrics. This year, our focus

lies in utilizing testing data for a more informed and targeted design. Using data from last year, we have identified key aspects of our pod's design that can be strengthened. For this year's pod, we have set a loose requirement of a 4-foot long, 11-inch wide, and 9-inch tall pod with a mass of 80kg. With these requirements, we have moved forward with a dual motor design to double our speed, a pneumatically actuated friction braking system that reduces the overall braking distance by 33%, and a redesigned power system that modulates power consumption.

To meet these design requirements, we are working on a new motor selection process using an internally developed trajectory simulation and redesigned suspension geometries. The stabilization team utilized MATLAB's Simulink to develop a multi-degree of freedom pod model based on derived equations of motion to select the best stabilization parameters. In parallel, the research and development team is designing and prototyping a Linear Induction Motor that will reduce friction losses and allow for much higher acceleration and top speed. Coupled with a redesigned braking system that increases the pod's deceleration to upwards of 3G's, we anticipate a trajectory with a top speed of 35 m/s on a 100m track. Moreover, electronics is working to support the team's endeavors through integrating robust protective circuitry and designing high speed-signal PCBs verified through programs like ANSYS ICEPAK and SI WAVE. Power Systems is also creating models through MATLAB that allows the team to understand the characteristics of high voltage systems and pinpoint our optimal design for speed and reduced power consumption. In tangent, the controls team is developing reliable communication networks that display all the pod's parameters on a graphical user interphase (GUI). This interphase will allow us to read values from all our sensors and control the pod remotely. An additional goal this year is displaying a 3D model of the pod that demonstrates the position and speed.

Success on our team encapsulates more than building a Pod. By designing for EHW, our team strives to improve each Pod that is built in subsequent years, whether that is increasing the top speed and acceleration, increasing the PCB efficiency, decreasing the braking distance, or any other technical requirement. With throughout documentation of current work, we hope that future years of the HyperXite team and other Hyperloop organizations are able to use our developments to help drive the future of Hyperloop technology.

Table of Contents

List of Figures

List of Tables

Chapter 1: Problem Definition

1.1 Background

The Hyperloop concept was proposed by Elon Musk in a 2013 white paper titled “Hyperloop Alpha”, which described a low-pressure system containing a track on which transport pods could travel [4]. Among other suggestions, a linear electric motor was described as the propulsion mechanism of choice. A linear induction motor (LIM) works on the same principles as rotary induction motors used in most modern electric vehicles, but produces linear rather than rotational motion. A LIM consists of a stator—a magnetically permeable core with coils powered by alternating current (AC) of multiple phases (usually 3 equally shifted)—and a rotor—an electrically conductive blade. The stator coils produce a magnetic field and induce Eddy currents in the rotor; the resulting magnetic and electric fields interact to produce a Lorentz force which provides linear acceleration.

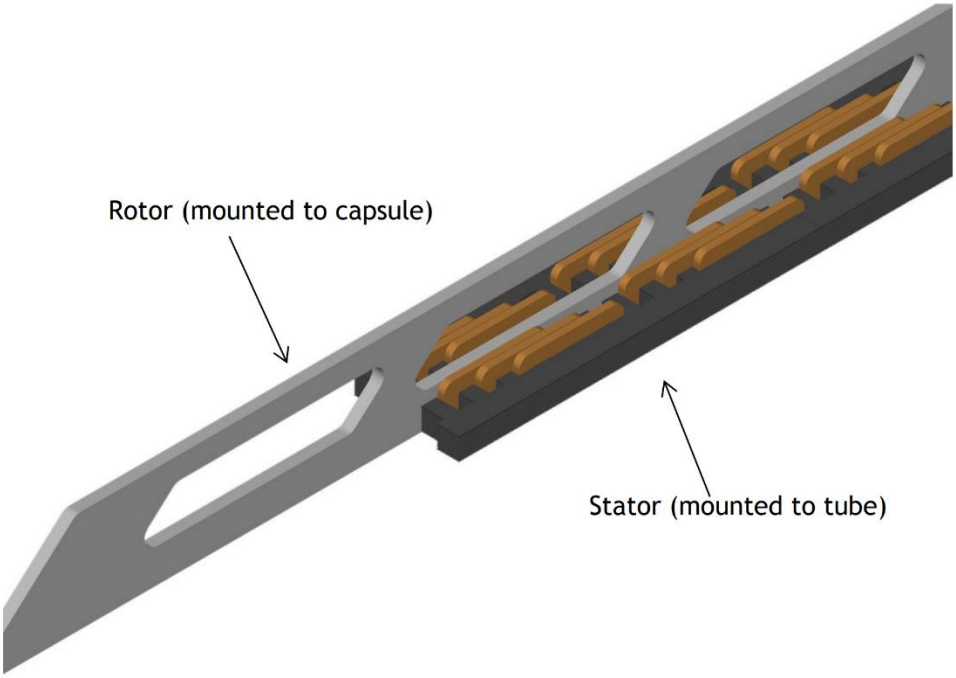

Figure 1. Short-secondary linear induction motor concept from Hyperloop Alpha.

1.2 Existing Design Solutions

A number of companies have been developing Hyperloop technologies in recent years, including Virgin Hyperloop and Hyperloop Transportation Technologies. Notably, Virgin Hyperloop achieved the first passenger test on their pod in November 2020. Unfortunately, not much is known about their proprietary technology, and their propulsion and levitation systems are especially kept

under wraps. Other university teams competing in Hyperloop competitions have developed their own linear induction motors and a few research papers have been published on the process [1].

1.3 Problem Statement

The Hyperloop pod requires a mechanism of providing propulsion to accelerate and maintain cruising speed. HyperXite's pods have historically used various types of rotary motors for wheel-based propulsion; our sub-team aims to develop HyperXite's first linear induction motor, as this is a critical technology to achieve Hyperloop's envisioned speed and efficiency. Using a linear induction motor for pod propulsion takes advantage of the provided conductive track and will enable future iterations to implement levitation. Since the track material and geometry are defined by the competition, we are limited to using a short-primary configuration, meaning the track acts as the rotor while the stator is mounted to the pod.

1.4 Design Attributes

Legend
O: Objective, **C**: Constraint, **F**: Function, **M**: Means

Table 1: Design Attributes

Attribute	**O**	**C**	**F**	**M**
Must propel the pod to at least 35 m/s			x	
Must accelerate and decelerate the pod in about 100 m			x	
Should be reasonable in mass such that the pod doesn't exceed a total mass of 80 kg		x		
Should be on both sides of the track (double-sided)	x			
Should be made of a magnetically permeably material				x
Should have 3 phases of AC current		x	x	
Should be less than 1.5 m long, 0.3 m wide, and 0.067 m tall for each side		x		
Should be powered by DC batteries with an inverter		x	x	
Should have two magnetic poles		x	x	
Should maintain an air gap between the track and each side of the LIM		x	x	
Should be a short-primary configuration	x			
Should adhere to track and pod design constraints		x		
Should be winded with many coils, maybe in parallel				x
Must not conduct electrical arcs through the air			x	

Must not waste magnetic flux in the core such that it is dissipated into heat			x	
Must meet regulations of the European Hyperloop Week competition		x		

1.5 Objectives and Requirements

Objectives-to-Requirements Tree

- HyperXite's LIM
    - The LIM needs a power source for its induction
        - Coils on the LIM must be used to generate induction of a magnetic field
        - Coils must have a 3-phase AC input with a 120° phase delay
        - Power needs to come from batteries where an inverter is needed to convert DC input to 3-phase AC output
    - The LIM must of a short-primary configuration
        - The LIM must be mounted to the pod
        - The LIM should be shorter than the track and be similar in length to the pod
        - The LIM must induce eddy currents in the track, which is of a long-secondary configuration
    - The LIM must be double-sided
        - The LIM must have two sides, each placed on either side of the track
        - The LIM must adhere to the track geometry and avoid the keep-out zones
        - The LIM must adhere to Hyperxite's pod constraints
        - An air gap between the track and both sides of the LIM should be maintained

1.6 Work Breakdown Structure

I. Project definition
    a. Define project scope
    b. Determine objectives and requirements
    c. Review existing design solutions
II. Preliminary research
    a. Understand the underlying physics concepts
    b. Literature review
    c. In-depth reading of the most relevant papers
    d. Narrow product scope
III. Initial design

a. Make design selections
b. Define specific constraints
c. Determine key parameters

IV. Optimization
a. Analytical model (Tae)
b. Simulation (Ethan)
c. Key parameter optimization

V. Final design
a. CAD
b. Electrical diagram
c. Bill of materials
d. Manufacturing plan

VI. Manufacturing and testing
a. Component machining
b. Assembly
c. Testing

1.7 Milestones and Deliverables

Table 2: Milestones and Deliverables

Task	**Start**	-	**End**
Rules and Regulation Review	7/11/21	-	7/13/21
Hyperloop Concept Background Review	7/14/21	-	7/17/21
Research Linear Induction Motor Principles	7/18/21	-	8/1/21
Objectives and Requirements Definition	7/21/21	-	7/28/21
Literature Review on LIMs	8/1/21	-	8/22/21
Literature Review Synthesis	8/22/21	-	9/12/21
Specific Constraints Definition	10/1/21	-	10/8/21
Key Parameter and Equation Definition	10/8/21	-	10/22/21
Simplified Analytical Model Development	10/23/21	-	11/12/21
Simplified Simulated Model Development	10/23/21	-	11/12/21
Parameterized Simulations of Key Parameters	11/13/21	-	11/30/21
Coupled Simulations of Key Parameters	12/1/21	-	12/12/21
Analytical Model Development of Prototype	1/3/21	-	1/10/21
Simulated Model Development of Prototype	1/3/21	-	1/17/21
CAD Model of Prototype	1/10/21	-	1/15/21
Electrical Diagram	1/15/21	-	1/30/21
Manufacturing Plan	2/1/21	-	2/20/21
Manufacturing and Testing	Winter 2022 & Spring 2022		

Chapter 2: Conceptual/Preliminary Design (Design of Key Components)

2.1 Key Components

In this section, we will discuss the preliminary design motivations for the rotor, stator core, stator winding, and power systems.

2.1.1 Rotor

Our LIM is a short-primary, so the rotor is a long electrically conductive track which the pod rides on. Since the track is provided at the European Hyperloop Week competition, this component has already been defined. The track used is a 6061-T6 aluminum I-beam with dimensions provided in the drawing below. The red regions are keep-out zones which must be left empty at all times. Therefore, the LIM must be designed such that it operates about the track and keep-out zones.

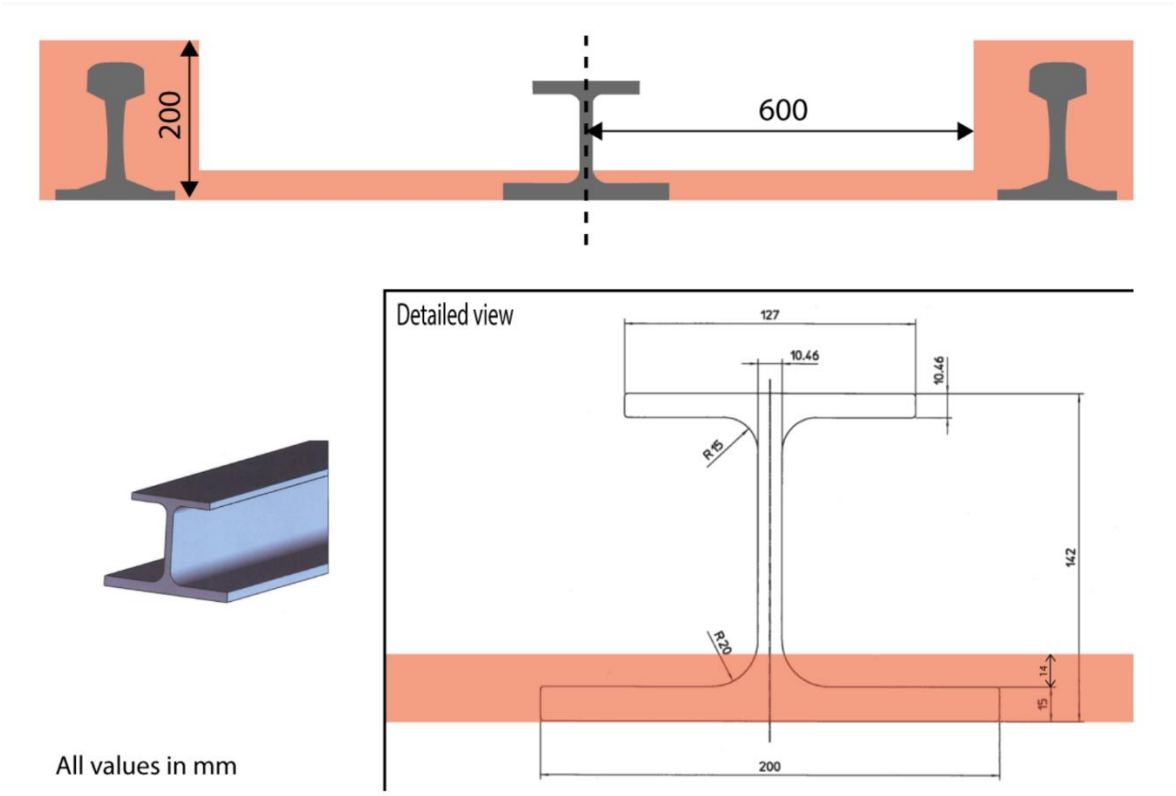

Figure 2. European Hyperloop Week track dimensions (mm).

2.1.2 Stator Core

The first design choice for the stator is between a single-sided and double-sided layout. Considering the given track geometry, a single-sided layout could be achieved by interfacing the stator with the top flange of the I-beam track, while a double-sided layout could be achieved by sandwiching 2 stators around the web of the I-beam track.

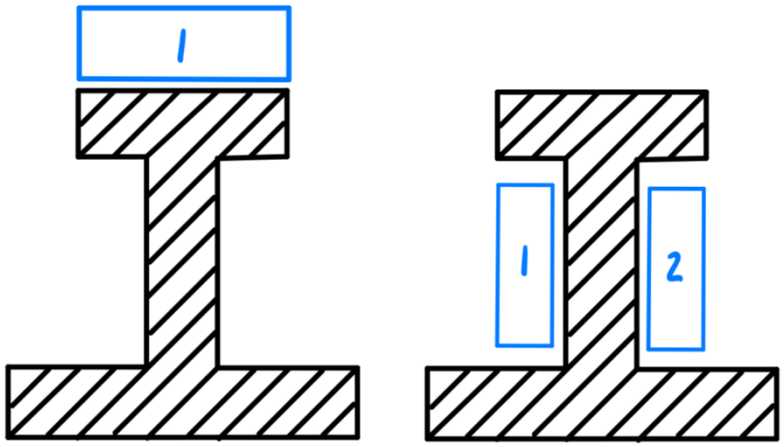

Figure 3. Single-sided layout (left) and double-sided layout (right).

The single-sided layout has the potential added benefit of providing lift for a levitation system, but the double-sided layout can achieve far higher efficiency as it reduces stray flux by coupling the generated stator magnetic field. Additionally, the double-sided layout is self-stabilizing in the lateral direction.

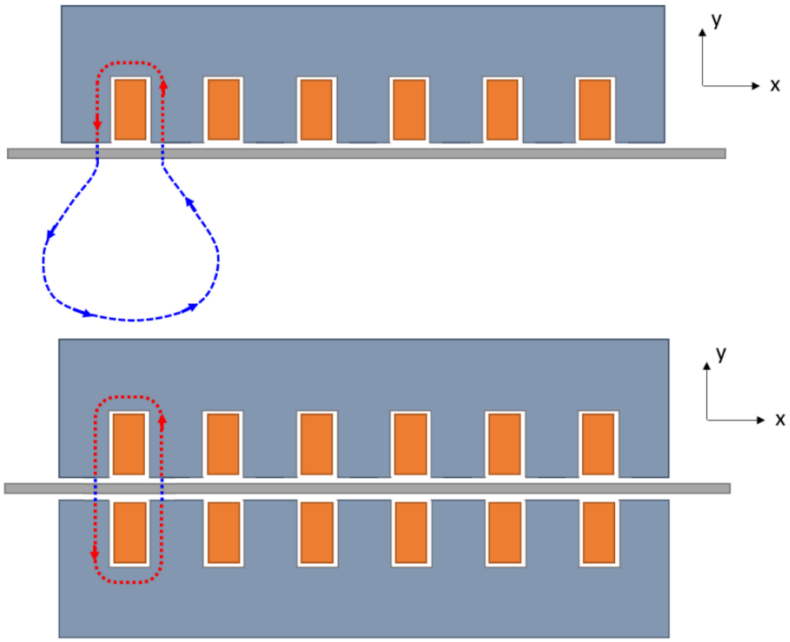

Figure 4. Flux path of single-sided layout (top) and double-sided layout (bottom) [1]

As figure 4 conveys, the flux path through air is much shorter in the double-sided layout, resulting in less losses. For this reason, and because we do not have plans for a levitation system at this point in time, we have opted for a double-sided layout.

The stator core is a magnetically permeable structure consisting of a yoke from which a number of teeth are extruded outwards with slots in between to house the coil windings. The purpose of the stator core is to concentrate and direct the magnetic flux produced by the coils through the air gap and rotor. AC is directed through the coil windings, which generates a magnetic field that induces eddy currents within the rotor. These eddy currents in turn induce an equal and opposite magnetic field. There exists a difference in speed of these fields, known as slip, such that this leads to an acceleration, and subsequently a force, that drives the stator along the rotor length.

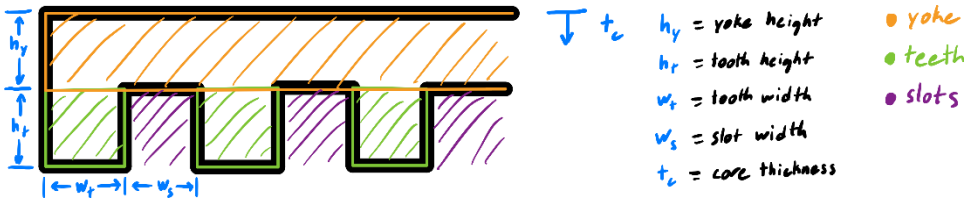

Figure 5. Stator core geometry and parameters.

Since the stator core must fit between the I-beam track flanges and abide by the defined keep-out zones, the core thickness must be less than 67mm. The cross-sectional area of the teeth and yoke (controlled by tooth width and yoke height, respectively) must be large enough so that the induced flux density does not exceed the saturation flux density of the core material. The slot size (controlled by slot width and tooth height) must provide enough room for the coil windings.

Magnetic flux takes the path of least reluctance, so the stator core material should be highly magnetically permeable in order to help constrain the field to the shape of the core and minimize losses related to reluctance. The shape of the core is optimized to minimize stray flux losses and increase useful flux that penetrates the rotor and generates magnetomotive force. Additionally, the material must have a high saturation flux density to increase the amount of flux for magnetomotive force generation. Soft iron-based materials such as silicon steel and manganese-zinc ferrite are typically used because they possess favorable property characteristics as stated above.

2.1.3 Stator Windings

The windings, or coils, of the stator induces a magnetic field through its center when current is passed through its wires. AC, a time-varying style of current that is usually sinusoidal in its magnitude, induces a time-varying magnetic field due to Ampere's Law, where the field is strongest near its amplitude and weakest in between them. It is desirable to have a system of uniform strength in order to generate a more consistent magnetic flux density, and thus a more

consistent Lorentz force, or thrust. To achieve this, phase-delayed input AC signals of equal amplitude can be added to the system such that any one phase can provide a maximum at any time. The most common approach to utilizing this multiphase excitation is with 3 inputs each separated by a phase delay of 120°, because more inputs lead to more complex designs and most LIM models have followed this approach.

The corresponding stator magnetic field generated by the 3-phase AC input must begin and end at itself due to Gauss's Law of Magnetism, such that a magnetic monopole cannot exist. This implies that poles develop in pairs. A lower number of pole pairs lead to less drag, which contributes to a higher thrust. Thus, for the most thrust, a pole number of 2 was selected. The geometric length of each pole, or pole pitch, can be manipulated by varying the core length or slot width to achieve higher thrust. The stator magnetic field translates linearly along the rotor length and interacts with the opposing magnetic field from the eddy currents that it has induced to generate motion.

With 3-phase AC input and its corresponding magnetic field, the number of slots per phase is integral in forming the sinusoidal shape of the stator magnetic field. Adding more slots to the stator core causes the stator field shape to become more sine-like and less n, but too many slots can lead to a more triangular waveform. Where the number of slots per phase influences the stator magnetic field, the number of turns per phase influences the eddy currents generated by the stator magnetic field. More turns lead to a higher induced stator voltage, which leads to stronger eddy currents. Thus, the resulting Lorentz force can be greater. Although, the number of turns used must fit within the size of the slot, maintain some spacing from the yoke, and be attached to the end of each tooth via some kind of support (i.e. a notch). Therefore, an optimal number of slots and turns must be selected based on size and material constraints.

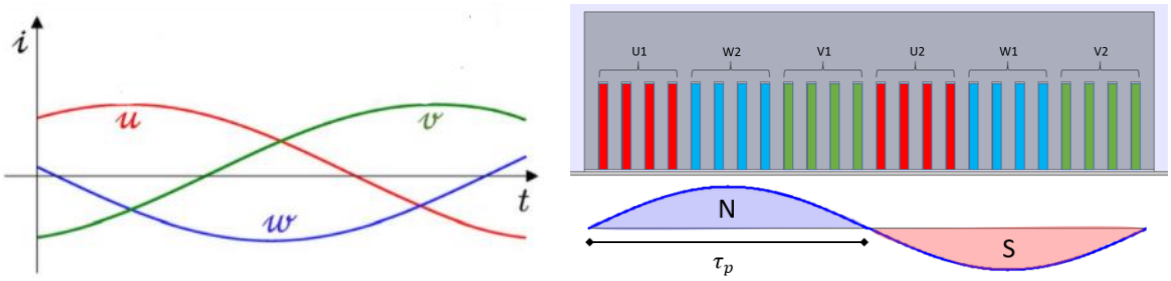

Figure 6. Example of a 3-Phase AC input LIM with its corresponding stator magnetic field, its north and south poles, and its pole pitch τp [1].

Copper wires will be utilized in the windings due to their high electrical conductivity, high thermal resistance, and inexpensiveness compared to other conductive materials. Copper wires come in different diameters, where larger diameters can withstand higher current values. The diameter of the copper wires will need to be selected based on the current amplitude passed through the windings, where the current amplitude is based on the magnetomotive force that fulfills the speed and force goals of the pod.

2.1.4 Power Systems

The coils will need to be powered by a 3-phase AC source with variable frequency. For this reason, we will need a converter to convert the DC power supply from the battery into this desired power source. A high-level component diagram is provided below.

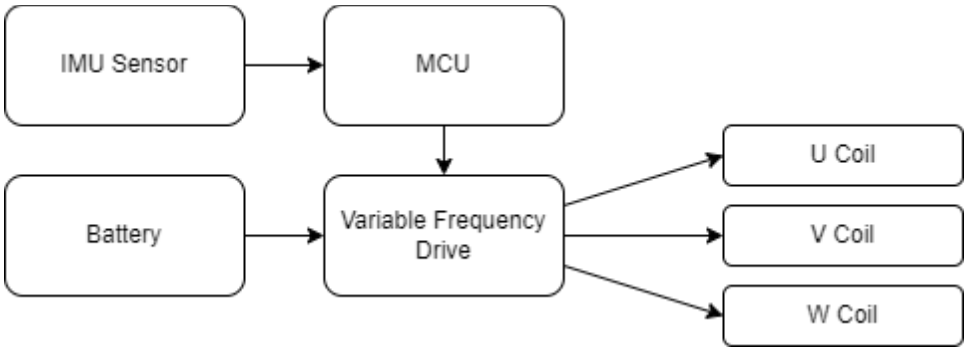

Figure 7. Preliminary high-level electrical component diagram.

We require a variable frequency drive because the optimal frequency changes with the pod's velocity. The thrust which accelerates the pod is a result of a delay between the rotor and stator fields called "slip". Slip is defined as the difference between the stator and rotor field velocities divided by the stator field velocity.

$$s = \frac{v_s - v_r}{v_s}$$

In the next chapter, we will describe how the optimal frequency can be chosen in order to maintain the slip value to optimize thrust throughout the pod velocity profile.

The coils are wired in a star connection such that the 3 phases all lead to a shared neutral wire. In the next chapter, voltage and current requirements for the coils will be determined. If there is only one wire for each phase, the total voltage requirement may turn out to be unreasonably high. In this case, we can reduce the voltage requirement while increasing the current requirement by using multiple wires connected in parallel for each phase.

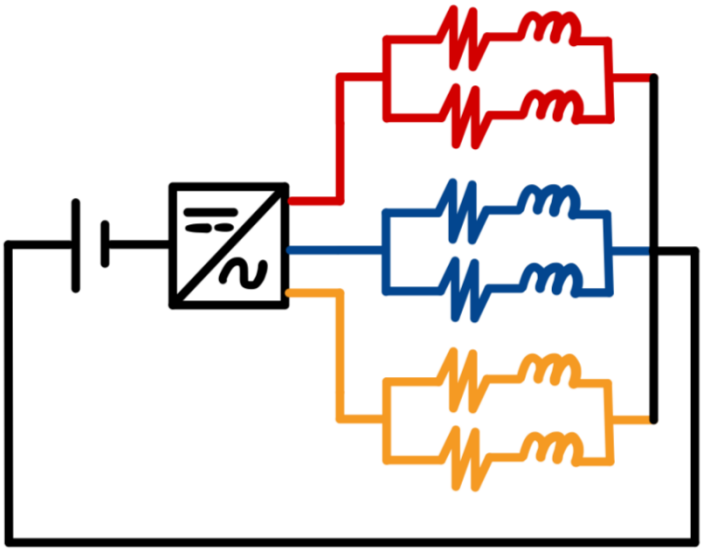

Figure 8. 3-phase star configuration with 2 parallel wires per phase.

The design of the battery setup and AC converter will be investigated once the magnetic flux density and eddy currents are defined by the stator core and coils setup.

2.2 Summary of Preliminary Design

Our LIM is required to be a short-primary, meaning that the stator core and windings are mounted to the pod and interact with the electrically conductive non-magnetic track. Additionally, we have chosen a double-sided configuration to achieve higher efficiency and self-stabilization. The stator core geometry and dimensions as well as the parameters of the winding configuration must be optimized to ensure the best magnetic field and eddy current generation given the design constraints, and speed and force goals. The following chapter will illustrate simulations that have led to the finalization of certain dimensional values.

Chapter 3: Detailed/Critical Design

3.1 Simulated LIM Model Formulation

Preliminary design involved understanding the stator core dimensions and winding configurations and how they relate to thrust generation for the Hyperloop pod. COMSOL Multiphysics, a finite element analysis software, was used to observe how changing parameters for an LIM affected the generation of thrust. However, these simulations were limited in scope due to flaws in the setup and mismatch of data with anticipated results. Therefore, to forego the testing of individual dimensions, a 2D model of an LIM was developed in COMSOL Multiphysics for more accurate and usable results. This model was verified by evaluating the thrust generated as mechanical velocity of the pod (v_r) (also known as the rotor field velocity) was varied from 0 up to the stator field velocity (v_s). This thrust vs. v_r curve was illustrated in [1] for their model, so by comparing the resultant curve for our 2D model with the curve in [1], similar-shaped curves demonstrated our model is accurate and usable for further simulations.

COMSOL Multiphysics does not have a dedicated LIM tutorial model, but they have similar electromagnetic motors within their tutorial library. I utilized aspects of the rotary induction motor and linear motor tutorial models toward the overall LIM simulation. Boundary conditions applied and physics conditions imposed were learned for each model. A mixture of different aspects of each tutorial model factored into the setup of the LIM in COMSOL Multiphysics. This comparative process was tedious, as a lot of trial and error had to be used to input correct conditions and extract the correct values. Eventually, the 2D LIM model was finalized after a few weeks. An image of the model and the notable variables are shown below.

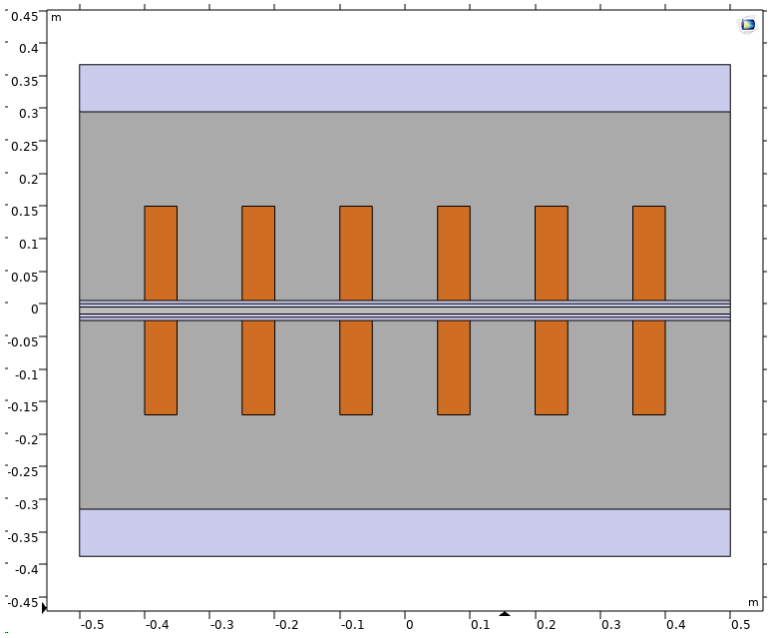

Name	Expression	Value	Description
L_LIM	100[cm]	1 m	LIM length = yoke length
T_LIM	30 [cm]	0.3 m	LIM thickness (b/t flanges)
slotnum	6	6	number of slots
w_s_max	L_LIM/slotnum	0.16667 m	maximum slot width allowed
wmult	0.5	0.5	slot width multiplier
w_s	wmult*w_s_max	0.083333 m	slot width
w_t	(L_LIM - slotnum*w_s)/(slotnum+1)	0.071429 m	tooth width
h_rotor	10.48 [mm]	0.01048 m	rotor web thickness
h_sr	10 [mm]	0.01 m	distance b/t one stator and rotor
g	h_rotor + 2*h_sr	0.03048 m	total distance b/t stators
h_stator	(2*30.48 [cm] - g)/2	0.28956 m	stator height (note: 1 ft = 30.48 cm)
hmult	0.5	0.5	tooth height multiplier
h_y	(1-hmult)*h_stator	0.14478 m	yoke height (note: from tooth length upward)
h_t	h_stator-h_y	0.14478 m	tooth height (note: also slot height)
I_coil	100 [A]	100 A	coil wire peak current
phaseang_i	0 [deg]	0 rad	initial current angle
A_coil	0.080 [mm^2]	8E-8 m^2	coil wire cross-section (note: AWG 28)
N	100	100	number of wire turns per phase
f_s	25 [Hz]	25 Hz	stator frequency
pnum	1	1	pole pair number
tau_p	L_LIM/(2*pnum)	0.5 m	pole pitch
v_s	2*tau_p*f_s	25 m/s	stator field velocity (sync speed)
v_r	0[m/s]	0 m/s	mechanical velocity (rotor field velocity)
sigma_rotor	3.030e7[S/m]	3.03E7 S/m	electrical conductivity of the rotor
mu_r	1.25663753e-6 [H/m]	1.2566E-6 H/m	permeability for air (free space and relative (material) permeability combined)

Figure 9. 2D LIM COMSOL Model and Variables

A slot number of 6 was chosen initially because this constitutes the most basic form of the LIM concept. Specifically in the model, the geometry of the stator core was inputted using variables such that numerical values can be swapped easily for future geometrical variations. Arbitrary values – notably LIM length, height, and width - were inputted within the constraints mentioned in Section 1. The *Magnetic Field* physics module was utilized to apply coil winding conditions for each phase and for specific slot pairings. Lastly, a parametric sweep was applied to evaluate the resultant force in the x-direction, which is the thrust. An analytical equation for the thrust, derived from the theory mentioned in [1], was also inputted within the simulation using the same variables to observe the difference between this result and the simulated results. The analytical equation is explicitly written as:

F_thrust = (18*((N*I_coil)^2))*T_LIM*h_rotor*L_LIM*(sigma_rotor*(v_s-v_r))/(((pi*g/mu_r)^2) + ((v_s-v_r)^2)*((sigma_rotor*h_rotor*tau_p)^2))

The final result from the COMSOL simulation is illustrated below.

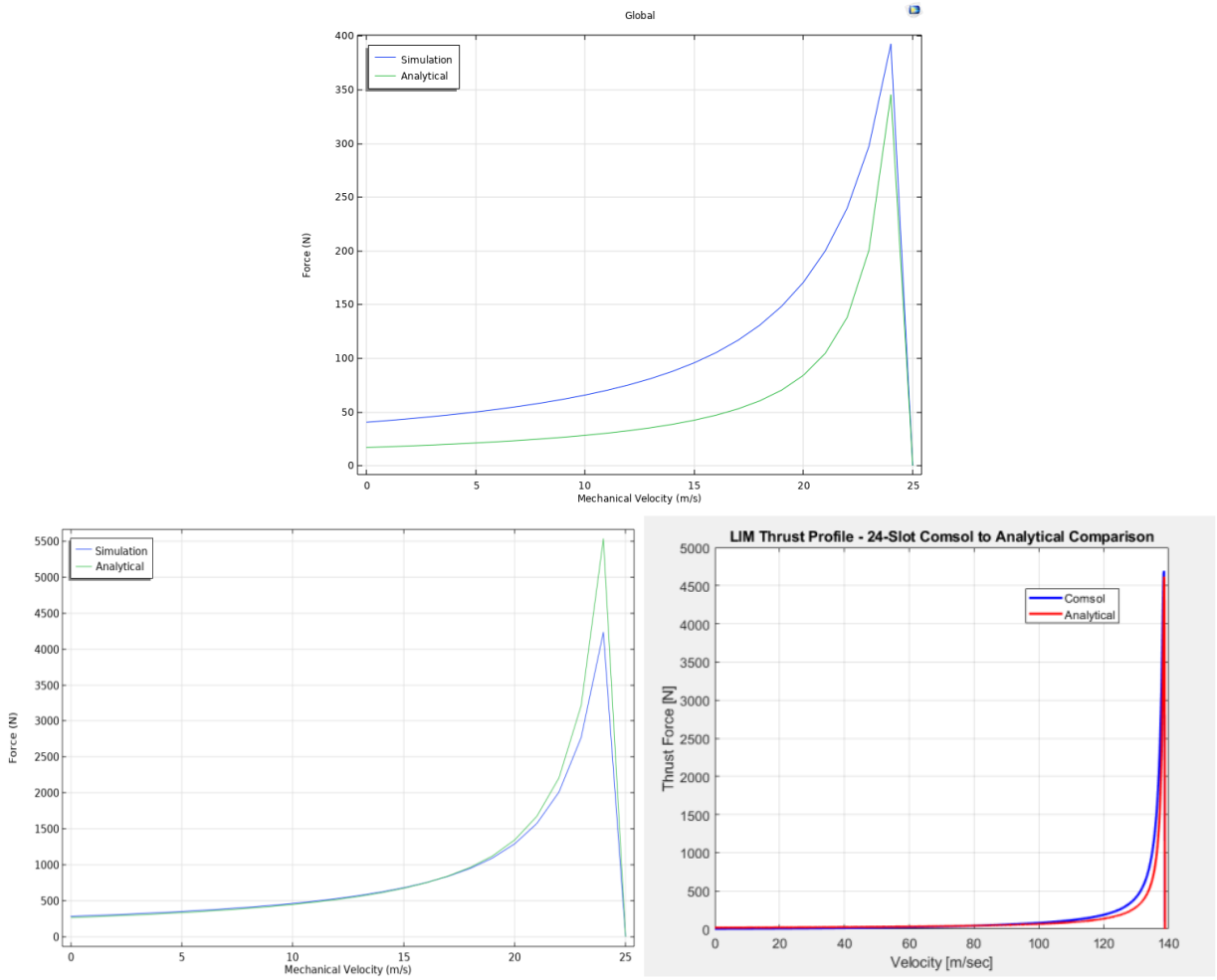

Figure 10. Thrust vs. Mechanical Velocity Curves for a self-developed 6-slot model (top), a self-developed 24-slot model (bottom left), and a 24-slot model from [1] (bottom right).

It is important to note that this initial model has 6 slots, and the thrust curves shown in [1] is for a 24-slot LIM model. After observing that the 6-slot model's thrust curve had the same shape as the curve in [1], a 24-slot model was simulated for more accurate comparison. The resulting curves from the 24-slot model is seen to resemble the curve in [1] much more, indicating that the self-developed 2D LIM model is valid for future simulations of its parameters and an accurate model for performance simulation.

3.2 Simulated LIM Model Parameterization

Knowing that the self-developed 24-slot model was verified in its accuracy based on comparison of the thrust curves with [1], experiments were planned to understand the different parameters of the 24-slot LIM. The first major experiment conducted involved understanding how changes in slot geometry affected the thrust performance of the LIM. For accurate experimentation, a few constraints were applied. First, all of the slots are set to be the same width, and all of the resulting teeth are also set to the same width as the slots. This meant that the LIM

length is purely a function of the slot width and slot number (which is defined as 24). The resulting equation is: (slotnum + 1)*w_t + slotnum*w_s = L_LIM. This yields a maximum slot width, which has an equation defined in Figure 9. Therefore, the slot width can be varied from just above 0 to just below the maximum slot width.

Because all the LIM dimensions are arbitrary, if thrust is evaluated based on different slot width values, these values are only pertinent to the specific LIM dimensions inputted. Therefore, it is important that this experiment yield results that can be applied to all other LIM dimension values even if some dimensions are arbitrary. A method to extrapolate these results for more significance is to nondimensionalize the parameters. For the slot width then in this case, the sum of the slot widths can be divided by the total LIM length to yield a slot width percentage. In other words, this percentage defines the amount of slot width per LIM length. Thus, if thrust is evaluated based on different slot width percentages, the relative position of different thrust values on the plot should correspond to a certain percentage, which would hold for any arbitrary LIM length.

This nondimensionalization is also helpful for other stator core dimensions. The second constraint applied is that all the slots are set to the same height. Like the slot width percentage, a slot height percentage can be defined, which is the slot height divided by the LIM height.

Other constraints involve the electrical energy applied to the LIM. These variables are listed in Figure 9, which involve coil wire cross-sectional area, number of turns per phase, peak current, pole pair number, and stator frequency. Other constraints also include the number of slots per phase and the number of turns per coil. The first variable is the quotient of the slot number and number of phases (which is 3), and the second variable is the quotient of the number of turns per phase and the number of phases.

With all the constraints defined for this experiment, the input parameters can be specified. A slot width multiplier term (“wmult”) and a slot height multiplier term (“hmult”) was each set from 0.05 to 0.95 at intervals of 0.05. The slot width multiplier term is a percentage of the maximum slot width, and because of the equation for the maximum slot width, the slot width multiplier term is also the percentage of total slot widths across the entire LIM length. Likewise, the slot height multiplier term is a percentage of the LIM height. Then, a parametric sweep was applied for these two inputs, specifically allocating for all possible combinations of the two terms, so that a model for each combination was created. After simulation, the thrust was calculated for each combination and plotted in MATLAB as seen below. The thrust is also nondimensionalized as a percentage of the maximum thrust in the entire simulation so that every point evaluated can be compared to the maximum thrust that can be produced out of the possible combinations. This is useful because other geometry combinations can yield thrust values that are close to the maximum and tradeoffs in thrust can be beneficial if some geometrical dimensions are changed to accommodate for heating, safety, or manufacturing restrictions.

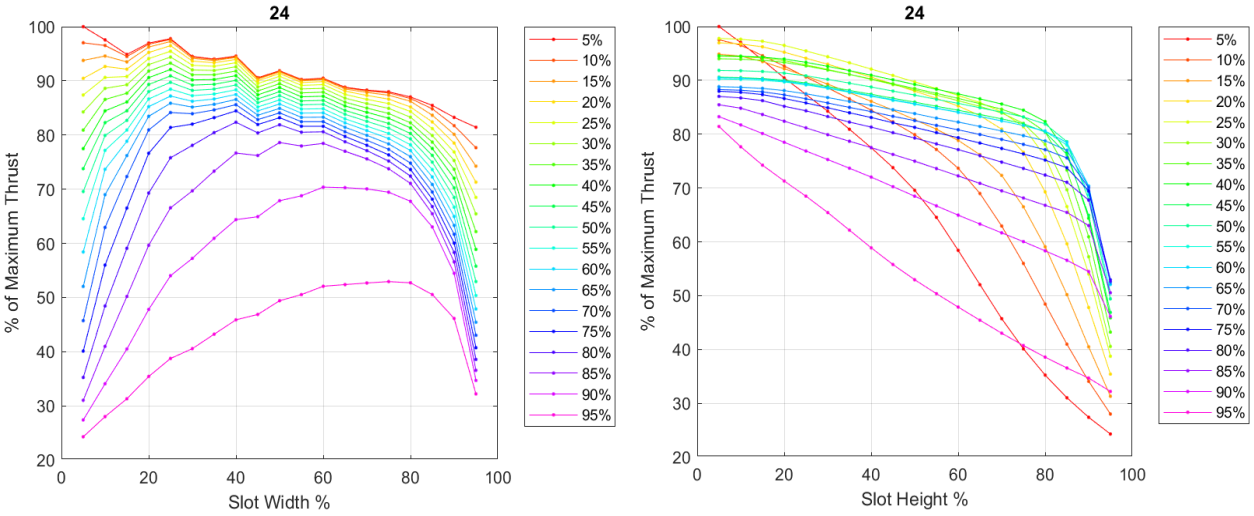

Figure 11. Percentage of Maximum Thrust versus Slot Width Percentage for varying Slot Height Percentages (left) and Percentage of Maximum Thrust versus Slot Height Percentage for varying Slot Width Percentages (right)

It is also interesting to observe how the slot area percentage (sum of total slot areas divided the LIM area) varies with maximum thrust percentage. This can be done because there is one thrust value for every slot width and slot height combination. The slot width and height percentages were utilized after simulation to derive a slot area percentage for every combination. The thrust percentage vs. area percentage can be seen below.

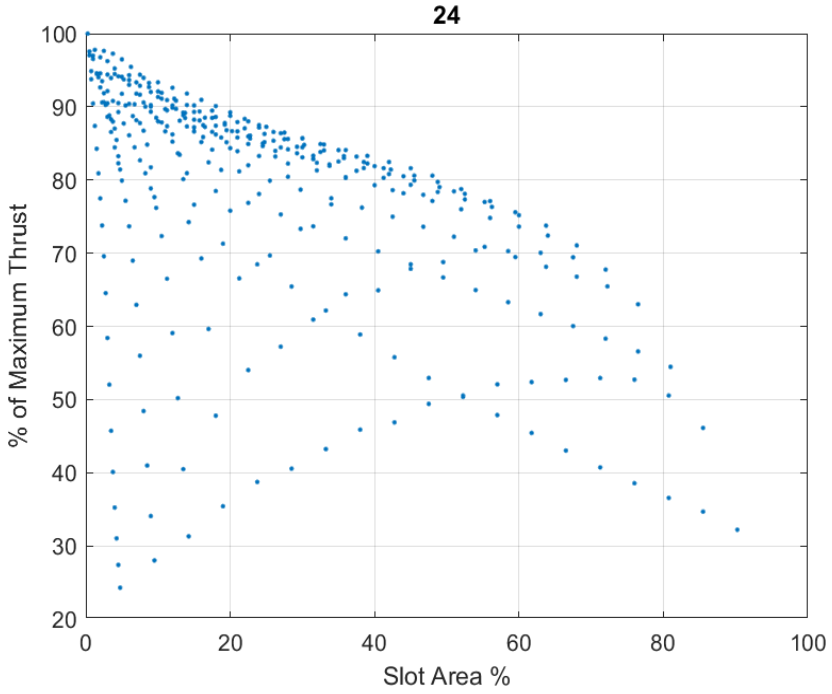

Figure 12. Maximum Thrust Percentage vs. Slot Area Percentage

3.3 Analytical Model

The main purpose of the analytical model is to understand the relationship between generated thrust, pod velocity, input voltage, and input frequency. We begin with this equation derived in [1]:

$$F = -\frac{72DL\Omega^2 d_r \mu^2 \sigma \left(v_r - v_s\right)}{L^2 d_r^2 \mu^2 \sigma^2 \left(v_r - v_s\right)^2 + 4g^2\pi^2}$$

Synchronous velocity, v_s, is a function of frequency:

$$v_s = \frac{L\omega}{2\pi}$$

Magnetomotive force, Omega, is simply the coil current times the turn number:

$$\Omega = IN$$

Additionally, we need a relationship between current and voltage because we can directly control voltage. For this, we will equate mechanical power with electrical power times the motor efficiency:

$$IV\eta = Fv_r$$

Putting all of these equations together, we have our final equation for thrust and velocity in terms of pod parameters and controllable inputs:

$$F = \frac{144DF^2LN^2 d_r \mu^2 \pi \sigma v_r^2 \left(L\omega - 2\pi v_r\right)}{V^2\eta^2 \left(L^2 d_r^2 \mu^2 \sigma^2 \left(L\omega - 2\pi v_r\right)^2 + 16g^2\pi^4\right)}$$

We can plot the relationship between thrust and velocity, leaving all other parameters constant.

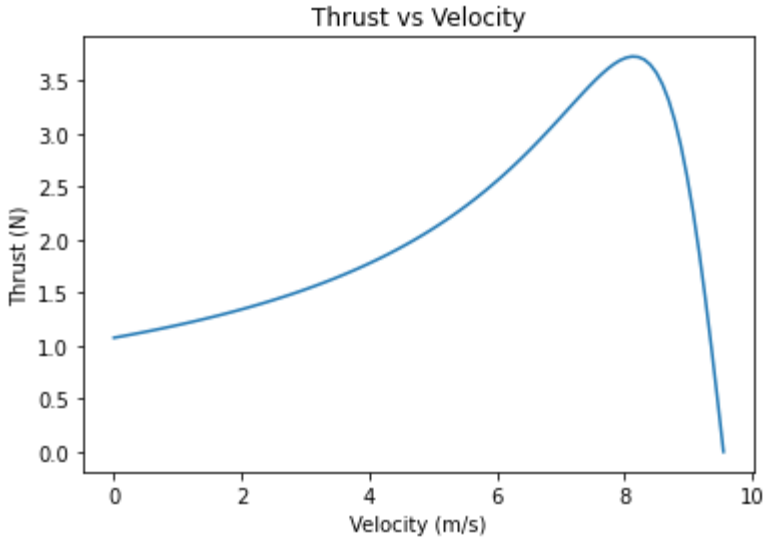

Figure 13. Thrust vs Velocity

Synchronous velocity is achieved at the far right of the curve, where velocity goes to zero, since no thrust can be produced when the rotor is traveling at the same speed as the magnetic field wave. The peak thrust is achieved just before the synchronous velocity. Since we can change the synchronous velocity by varying frequency, we are able to control where the peak thrust occurs. Additionally, we can control the magnitude of the peak thrust value by adjusting voltage.

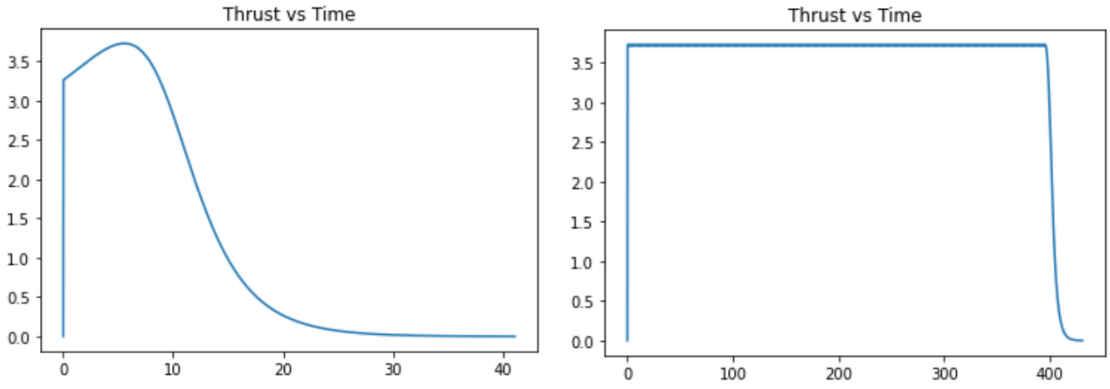

Figure 14. Thrust vs Time at constant frequency (left) and optimized frequency (right)

By linearly increasing frequency with respect to time, we can achieve constant maximum thrust. Constant thrust is achieved with constant current, but since the total power output increases at higher velocities, the voltage must be linearly increasing as well. The slope of the voltage curve corresponds with the magnitude of thrust, while the maximum value (determined by the battery) corresponds with the maximum cruising velocity of the pod.

3.4 Travelling Magnetic Wave

The purpose of the stator is to generate a travelling magnetic wave in the shape of a sinusoid. It is important that the shape is a sinusoid, because any deviations into higher harmonics results in turbulence and drag [1]. A perfect sinusoid is practically impossible to achieve, since we are constrained by manufacturability and dimensions. The ideal sinusoidal shape is achieved with infinitely many slots per phase and slot shifts, which is of course not feasible. However, we can plot the resulting magnetic fields of various configurations in order to identify a satisfactory middle ground between simplicity and efficiency.

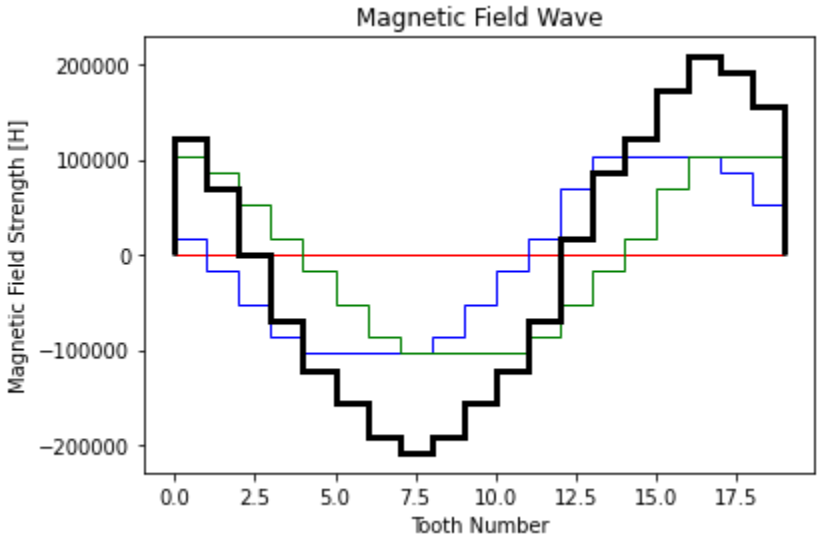

Figure 15. Resulting magnetic field wave from 3 slots-per-phase and 1 slot shift

Due to the dimensional constraints of our test rig, we have decided that a stator with 3 slots-per-phase and winding configuration of 1 slot shift will be satisfactory for the initial prototype. In the future, a refined LIM that will be integrated onto the full pod will likely have more slots-per-phase and potentially more slot shifts as well.

Chapter 4: Prototype Performance and Final Design

4.1 Initial Prototype Design

Taking all the theory and simulation that has been researched, we planned to build a proof-of-concept (POC) double-sided LIM model to test on a previously manufactured aluminum flywheel. This will demonstrate our understanding of the LIM and provide a baseline for future

iterations to improve upon. Experimental testing can be calculated to determine the LIM's performance and areas of improvement.

The aluminum flywheel has an outer diameter of 20 in. and an inner diameter of 2.25 in. To prevent the LIM from interfering with the center hole, a no-go zone will extend from the hole to have a diameter of 5 in. The thickness of the flywheel is 0.438 in., which will be the thickness of the rotor. Based on these dimensions, the LIM length and thickness were chosen such that the largest LIM could fit entirely within the flywheel dimensions. The figure below shows the final representation of these dimensions on the flywheel, where the LIM has a length of 12 in. and a thickness of 4 in. Also, a LIM height of 4 in. was chosen. A CAD model was also developed with arbitrary slot area dimensions to showcase its structure.

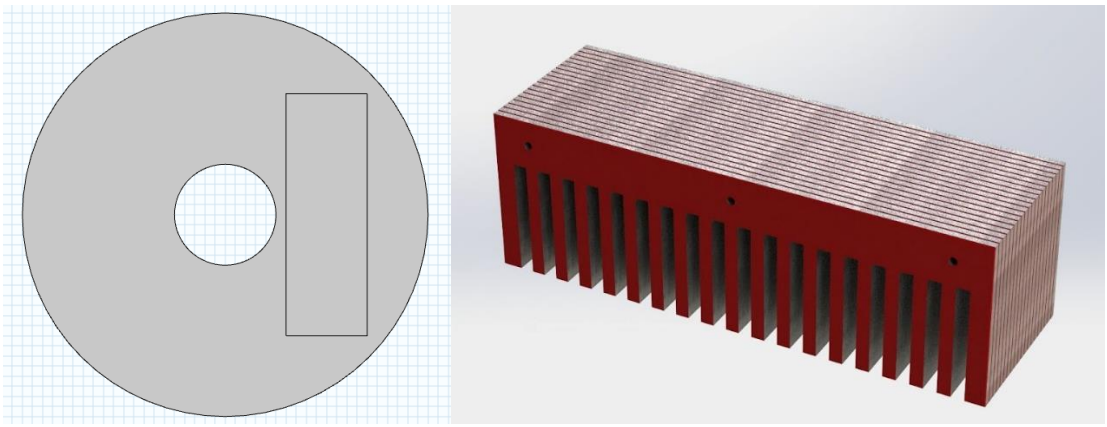

Figure 16. Top-Down View of the POC Double-Sided LIM on the Aluminum Flywheel (left) and a 3D Isometric View of the POC Double-Sided LIM (only one-side is shown) (right)

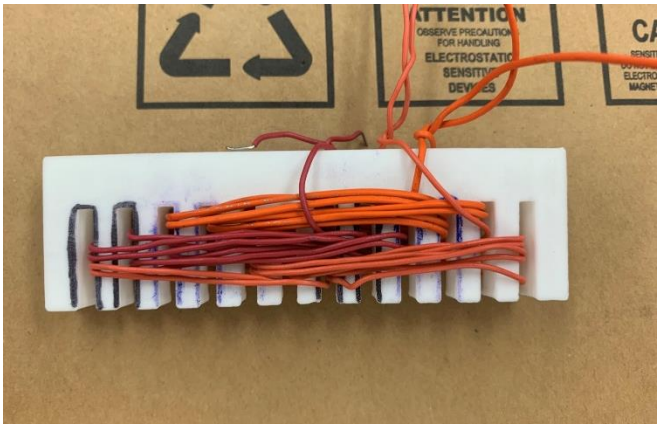

Figure 17. A 3D printed stator model with 3 slots-per-phase and 1 slot shift

After determining these dimensions, a slot area needed to be selected such that our POC can obtain the largest thrust. Because of the smaller size that the simulation (and also in [1]) and because this would be our first model, we scaled back on some of the previous electrical constraints mentioned in the simulation. Mainly, our POC will have 3 slots per phase with 90 turns per phase.

This will create 18 total slots, with 30 turns per slot pair. In addition, we will also utilize a technique mentioned in [1] called slot shifting, where some of the turns meant for one slot pair will be shifted to its adjacent slot pair, and the adjacent slot pair will also shift, etc. Specifically, we will take half of the turns per slot pair, so that 15 turns will stay in their original slot pair, and 15 turns will shift. This will create an offset in the phasing but should lead to a better distribution of the power such that the magnetic field wave will be smoother, which leads to higher thrust. In the following simulation, the slot shift will not be accounted for, as it is very complex to implement, but the other parameters will be adjusted from the 24-slot model to develop a comparative 18-slot LIM model.

After these parameters were changed and an 18-slot LIM model was developed in COMSOL, a code was created to determine what would be the ideal slot area size for our specific POC dimensions. Since the slot area should be minimized, it is only constrained by the size and number of coil wires. We first calculated the required wire gauge base on the wire current. From this, we can get the total wire cross-sectional area given the slot turn number (the number of wires going through each slot). Since the windings cannot be perfectly compact due to the physical constraints of winding, the fill area is divided by a somewhat arbitrary fill-ratio (which will be determined by test windings on 3D printed stators) in order to determine the slot area.

With an ideal slot area of 0.00041837 m^2, the total area of the slots was calculated, and an area percentage (total slot area divided by LIM area) of 12.16% was determined. Slot width percentage and slot height percentage simulations were repeated for the 18-slot model, and an area percentage was determined for each width and height percentage combination. Based on the intervals chosen, area percentages in the simulation came in intervals of 0.25%, so an area percentage of 12.00%, 12.25%, and 12.50% were sought after. Using MATLAB, code was developed to seek these area percentage combinations and extract the corresponding slot width percentage and slot height percentage. And because the LIM dimensions are known, the slot width and slot height values are known as well. Multiple tables are shown below regarding this process.

Table 3: 18-Slot POC Dimensions

slotnum	18	
L_LIM	0.3048	m
h_stator (1 side)	0.1016	m
h_stator (2 side)	0.2032	m
A_stator (1 side)	0.03096768	m^2
A_stator (2 side)	0.06193536	m^2
w_s_max	0.01693333	m
A_1slot	0.00041837	m^2
A_1slot	4.18369664	cm^2
A_allslots	0.00753065	m^2
A%	12.16%	

Table 4: 18-Slot LIM Model Values Corresponding to the Chosen Slot Area

Slot Area %	Slot Width [m]	Slot Height [m]	Thrust % of Maximum	Slot Width %	Slot Height %
12%	0.0034	0.061	79.65%	20.00%	60.00%
	0.0051	0.0406	93.21%	30.00%	40.00%
	0.0068	0.0305	91.90%	40.00%	30.00%
	0.0102	0.0203	89.15%	60.00%	20.00%
12.25%	0.0059	0.0356	93.07%	35.00%	35.00%
12.5%	0.0042	0.0508	88.76%	25.00%	50.00%
	0.0085	0.0254	91.26%	50.00%	25.00%

These values listed in Table 4 showcase the possible width and height combinations for the slot area of the POC. Future work will involve selecting a specific combination to move forward with manufacturing. After a combination is selected, more research in the power supply for the POC will be investigated and a set plan for winding the coils will be determined.

Chapter 5: Design Recommendations and Conclusions

Last quarter, we thoroughly researched the physics behind an LIM and how it is designed. We defined key aspects of the LIM, how these aspects contribute to the thrust, and their design goals and constraints. Over the course of this quarter, we used this knowledge to develop simulation and analytical models for a double-sided LIM. We defined design constraints for a proof-of-concept LIM prototype and used our new models to optimize the dimensional parameters of the stator core. In the next quarter, we will work with partners to manufacture the POC prototype for testing and analysis. Additionally, we will continue to refine our models and optimize other aspects of the LIM.

Acknowledgements

We would like to express our gratitude to Professor Roger Rangel, for your support and guidance as HyperXite's project advisor, and Professor Camilo Velez Cuervo, for sharing your time and knowledge on electromagnets.

References

[1] Timperio, Christopher. *Linear Induction Motor (LIM) for Hyperloop Pod Prototypes*. ETH Zurich. 2018.
[2] Furlani, Edward P. *Permanent Magnet and Electromechanical Devices*. Eastman Kodak Company. 2001.
[3] *European Hyperloop Week 2022 Rules and Regulations*. 2.1. European Hyperloop Week. November 16 2021.
[4] Musk, Elon. *Hyperloop Alpha*. Tesla Inc. 2013.

Appendix

A.1 LIM Model JSON

```
{
    "prototype_1":
    {
        "pod_mass": 100,
        "stator_width": 0.1016,
        "stator_length": 0.3048,
        "rotor_thickness": 0.0111252,
        "gap": 0.02,
        "slots_per_phase": 3,
        "parallel_number": 4,
        "turns": 4,
        "slot_shifts": [0,1],
        "operating_current": 100,
        "max_voltage": 200,


        "thrust_factor": 0.9,
        "rotor_conductivity": 2.857e8,
        "air_permeability": 1.25663753e-6,
        "motor_efficiency": 0.93,
        "slot_fill_ratio": 0.6,
        "slot_aspect_ratio": 0.125
    }
}
```

A.2 Slot Dimensions Calculation

```
# Imports
import json
import os
from math import pi, sqrt, sin
from collections import namedtuple
import matplotlib.pyplot as plt
import matplotlib.animation as animation
import pandas as pd

# Unpack LIM Data
```

```
data_file_name = 'data/lim_data.json'
lim_name = 'prototype_1'
save_to_folder = f'analysis/{lim_name}'

if not os.path.exists(save_to_folder):
    os.makedirs(save_to_folder)

with open(data_file_name) as file:
    data = json.load(file)
    lim = data[lim_name]

# Calculations
POLE_NUMBER = 2 # 2 poles
PHASE_NUMBER = 3 # 3 phases
STATOR_NUMBER = 2 # 2 stators (double-sided)

lim['pole_pitch'] = lim['stator_length'] / POLE_NUMBER
lim['turn_number']   =   lim['slots_per_phase']   *   lim['parallel_number']   *
lim['turns'] * len(lim['slot_shifts'])
lim['wire_current'] = lim['operating_current'] / lim['parallel_number']
lim['mmf'] = STATOR_NUMBER * lim['turn_number'] * lim['wire_current']
lim['max_thrust']   =   (18   *   lim['stator_width']   *   lim['mmf']**2   *
lim['air_permeability']) / (pi * lim['gap'])
lim['operating_thrust'] = lim['thrust_factor'] * lim['max_thrust']
lim['max_velocity']  =  (lim['motor_efficiency']  *  lim['operating_current']  *
lim['max_voltage']) / (lim['operating_thrust'])

lim['slot_number'] = lim['slots_per_phase'] * PHASE_NUMBER * POLE_NUMBER
lim['tooth_number'] = lim['slot_number'] + 1
lim['magnetic_field_strength'] = lim['mmf'] / (2 * lim['gap'])

Gauge = namedtuple('Gauge', ['standard', 'diameter', 'ampacity'])

# Unpack Wire Gauge Data
gauges = []
gauge_data_file_name = 'data/wire_gauge_data.csv'
with open(gauge_data_file_name, 'r') as gauge_data:
    for line in gauge_data.readlines():
        standard, diameter, ampacity = line.strip().split(',')
        gauges.append(Gauge(standard, float(diameter)/1000, float(ampacity)))

# Determine Required Wire Gauge
def find_best_gauge(current):
    best_gauge = gauges[0]
```

```
    for gauge in gauges:
        if    (1.5*gauge.ampacity    >=    current)    and    (gauge.ampacity    <
best_gauge.ampacity):
            best_gauge = gauge
    return best_gauge

best_gauge = find_best_gauge(lim['wire_current'])
lim['wire_gauge'] = best_gauge.standard
lim['wire_diameter'] = .003264# best_gauge.diameter

# Determine Required Slot Dimensions
wire_area = pi*(lim['wire_diameter']/2)**2
fill_area = lim['turns']*lim['parallel_number']*len(lim['slot_shifts'])*wire_area
slot_area = fill_area / lim['slot_fill_ratio']

lim['slot_height'] = sqrt(slot_area/lim['slot_aspect_ratio'])
lim['slot_width'] = lim['slot_height']*lim['slot_aspect_ratio']

# Determine Required Tooth Dimensions
lim['tooth_width'] = (lim['stator_length'] - lim['slot_number']*lim['slot_width'])
/ lim['tooth_number']
```